

# Polarizability and single particle spectra of two-dimensional s- and d-wave superconductors

Hae-Young Kee<sup>1,2</sup> and C. M. Varma<sup>2</sup>

<sup>1</sup> *Department of Physics, Rutgers University, Piscataway, NJ 08855-0849*

<sup>2</sup> *Bell Laboratories, Lucent Technologies, Murray Hill, NJ 07974*

## Abstract

We present analytic results for the polarizabilities,  $\chi(\mathbf{Q}, \omega)$ , in the charge, spin, and current channels for two-dimensional s- and d-wave superconductors for large momentum transfer. A collective mode in the charge channel is predicted to exist for extremum vectors of the Fermi-surface with energy below twice the maximum superconducting gap. Such modes are directly observable through inelastic x-ray or electron scattering. Scattering of single particle excitations by these collective modes leads to several unusual features in the single particle spectrum in the superconducting state which are seen in angle resolved photoemission experiments.

PACS numbers: 74.20.-z, 74.20.Fg, 74.25.Nf

## I. INTRODUCTION

It is now well established that the hole doped cuprates superconductors are d-wave superconductors with a very strong two-dimensional anisotropy. [1] It is clear that electron-electron interactions lead to the attractive pairing, although no consensus has emerged about the precise physical nature of such interactions. These interactions must also produce a very unusual spectra of particle-hole fluctuations leading to the observed non-Fermi-liquid transport properties in the normal metallic state, at least, near the hole-density for maximum  $T_c$ .

A phenomenological model [2] from which many of the anomalous transport properties can be calculated consistently assumes that the particle-hole fluctuations are scale-invariant, as in the critical region of a quantum phase transition. This model further assumes that the fluctuations are nearly momentum independent, leading to the prediction that the single-particle scattering rate – measurable in angle resolved photoemission(ARPES) or tunneling spectra – has the same anomalous temperature(and frequency) dependence as in the momentum scattering rate measured through the resistivity or the energy scattering rate measured by thermal-conductivity. The prediction of an unusual single particle line shape was verified by ARPES experiment. [3]

Any particle-hole spectra, usual or unusual, must develop a gap related to the superconducting gap below  $T_c$ . If the lifetime of quasi-particles in the normal state is primarily determined by electron-electron interactions, it must become very long in the superconducting state compared to the extrapolation from the normal state. [4] This prediction has been also verified. [5] A further prediction followed from the realization that the particle-hole spectra must revert to its normal state form at energies well above twice the (maximum) superconducting gap. Therefore quasi-particle line shape for energies above about  $3\Delta$  must continue to be of the normal state form. The single-particle spectrum in the superconducting gap must then be a sharp peak near the BCS energy followed by a broad hump starting at about  $3\Delta$ . [6] These predictions have been also qualitatively verified through ARPES

spectra. [7–9]

Recent more precise ARPES measurements [10,11] have motivated us to examine more precisely the change in the particle-hole spectra and the single particle spectra in the superconducting state. The ARPES spectra shows a slower variation with  $\epsilon_{\mathbf{k}}$  of the sharp peak than BCS and a more robust hump near  $3\Delta$  than expected. Also, the calculations must be performed using the d-wave anisotropy of the gap rather than the s-wave gap used in the simple calculation performed earlier [6].

To obtain the single particle spectra, we must calculate the polarizabilities for the charge, current and spin channels as a first step. We expect that the momentum-dependence of the polarizability of d-wave superconductors would be qualitatively different from that of s-wave superconductors. The result for the polarizability of s-wave superconductors, at large momentum for both two and three dimensions (and the associated anomalies in the phonon spectra), were presented earlier. [12–14] We include the results for polarizability of s-wave superconductors, to compare with d-wave superconductors. For a spherical Fermi-surface in three dimensions, the lowest order polarizability in charge channel has a logarithmic singularity at energy  $2\Delta$  for momentum close to the extremum vector spanning the Fermi-surface,  $(2k_F, 0, 0)$ . In two dimensions the logarithmic singularity is present near momentum  $(k_F, k_F)$  but for momentum close to  $(2k_F, 0)$ , the singularity is stronger  $\sim (\omega - 2\Delta)^{-1/4}$ . We give further mathematical details in the Appendix A.

The singularities in the superconducting state in the polarizabilities at large momentum, (while they are absent in the normal state) arise because the singularity in the one particle density of states in BCS-superconductors near  $\Delta$  are strong enough to lead to singularities in the joint particle-hole densities of states at special momentum-vectors connecting points on the Fermi-surface. In the d-wave case, these will be vectors connecting points on the Fermi-surface with the maximum gap. Taking these points to be along the x and the y-axes in two-dimensions, see Fig. 1, we can define two vectors  $\mathbf{Q}_0$  and  $\mathbf{Q}_a$ .

$$\epsilon_{\mathbf{k}-\frac{\mathbf{Q}_0}{2}} = -v_F k_x + \frac{k_y^2}{2m_{\perp}},$$

$$\epsilon_{\mathbf{k}-\frac{\mathbf{Q}_0}{2}+\mathbf{Q}_a} = v_F k_y + \frac{k_x^2}{2m_\perp}. \quad (1)$$

$\mathbf{Q}_0$  will often be called the extremum vector. For an isotropic Fermi-surface, or more generally with a Fermi-surface of a square lattice we can interchange x and y in Eq.(1).

We find that no nesting is required for the singularities. However nesting, i.e.,  $\frac{1}{m_\perp} = 0$  for points of the Fermi-surface (coincident with the maximum of the gap for the d-wave case ) leads to stronger particle-hole singularities.

The most important new result in this paper is that the particle-hole spectra in two-dimensions has a singularity at energy below  $2\Delta$  at large momentum transfer in charge channel in d-wave superconductors leading to new collective modes. Such collective modes can be observed directly by inelastic x-ray or electron scattering. Thus the particle-hole spectra does not just develop a gap below  $2\Delta$  as earlier assumed. [6] These results are true even when the normal state is a Fermi-liquid.

The collective modes also strongly influence the single particle spectra measured by ARPES. We compute the modified single-particle spectral function through the self energy near the maximum gap. We find a sharp peak near  $\Delta$  coming from the original BCS form and the broad hump below  $3\Delta$  arising from the exchange self energy due to the collective mode.

This paper is organized as follows. We first define the model and show the general formula for various response functions in section II. We also discuss the effect of the coherence factors in this section. We present analytical(and graphical) results of calculations of polarizabilities for both s-wave and d-wave superconductors, in section III and IV, respectively. In section IV, we also show single particle spectral function and compare with the experiment. In section V, we discuss the predictions, limitation of our results and comparison with existing experiments.

## II. MODEL AND DEFINITIONS

We consider the simplest possible model for the electronic energy

$$\epsilon_{\mathbf{k}} = \frac{k_x^2}{2m} + \frac{k_y^2}{2m} - \mu, \quad (2)$$

where  $\mu$  is the chemical potential,  $k_F^2/(2m)$ , in a circular Fermi-surface of radius  $k_F$  shown in Fig. 1. Any model with nesting on the Fermi-surface will have more singular polarizability than the isotropic surface, Eq. (2). We shall mention the expected corrections for such a case.

The single particle Green's function in the superconducting state can be written in the Gorkov-Nambu notation as [15]

$$G(\mathbf{k}, \omega) = \frac{\omega I + \epsilon_{\mathbf{k}}\tau_3 + \Delta_{\mathbf{k}}\tau_1}{\omega^2 - E_{\mathbf{k}}^2 + i\eta}, \quad (3)$$

where  $E_{\mathbf{k}}^2 = (\epsilon_{\mathbf{k}}^2 + \Delta_{\mathbf{k}}^2)$ . and  $\Delta_{\mathbf{k}} = \Delta$  for s-wave superconductor and  $\Delta_{\mathbf{k}} = \Delta \cos(2\phi)$  for d-wave superconductor.

The lowest order polarizability in charge, spin and current channels at momentum  $\mathbf{Q}$  and energy  $\omega$  are given at  $T = 0$  by

$$\chi_0^{charge}(\mathbf{Q}, \omega) = -i \int \frac{d^2k d\omega'}{(2\pi)^3} Tr[\tau_3 G(\mathbf{k} + \mathbf{Q}, \omega + \omega') \tau_3 G(\mathbf{k}, \omega')], \quad (4)$$

$$\chi_0^{spin}(\mathbf{Q}, \omega) = -i \int \frac{d^2k d\omega'}{(2\pi)^3} Tr[G(\mathbf{k} + \mathbf{Q}, \omega + \omega') G(\mathbf{k}, \omega')]. \quad (5)$$

$$\chi_{0,ij}^{current}(\mathbf{Q}, \omega) = -i \frac{e^2}{m^2} \int \frac{d^2k d\omega'}{(2\pi)^3} (\mathbf{k} + \mathbf{Q}/2)_i (\mathbf{k} + \mathbf{Q}/2)_j Tr[G(\mathbf{k} + \mathbf{Q}, \omega + \omega') G(\mathbf{k}, \omega')]. \quad (6)$$

where  $\tau_i$  are Pauli matrices.

After performing the frequency integral, they are given by

$$\chi_0^{charge}(\mathbf{Q}, \omega) = -\frac{1}{2} \sum_{\mathbf{k}} \left( 1 - \frac{\epsilon_{\mathbf{k}+\mathbf{Q}} \epsilon_{\mathbf{k}} - \Delta_{\mathbf{k}+\mathbf{Q}} \Delta_{\mathbf{k}}}{E_{\mathbf{k}+\mathbf{Q}} E_{\mathbf{k}}} \right) \left( \frac{1}{\omega + E_{\mathbf{k}+\mathbf{Q}} + E_{\mathbf{k}} + i\eta} - \frac{1}{\omega - E_{\mathbf{k}+\mathbf{Q}} - E_{\mathbf{k}} + i\eta} \right) \quad (7)$$

$$\chi_0^{spin}(\mathbf{Q}, \omega) = -\frac{1}{2} \sum_{\mathbf{k}} \left( 1 - \frac{\epsilon_{\mathbf{k}+\mathbf{Q}} \epsilon_{\mathbf{k}} + \Delta_{\mathbf{k}+\mathbf{Q}} \Delta_{\mathbf{k}}}{E_{\mathbf{k}+\mathbf{Q}} E_{\mathbf{k}}} \right) \left( \frac{1}{\omega + E_{\mathbf{k}+\mathbf{Q}} + E_{\mathbf{k}} + i\eta} - \frac{1}{\omega - E_{\mathbf{k}+\mathbf{Q}} - E_{\mathbf{k}} + i\eta} \right) \quad (8)$$

$$\chi_{0,ij}^{current}(\mathbf{Q}, \omega) \propto \frac{1}{2} \sum_{\mathbf{k}} (\mathbf{k} + \mathbf{Q}/2)_i (\mathbf{k} + \mathbf{Q}/2)_j \left( 1 - \frac{\epsilon_{\mathbf{k}+\mathbf{Q}} \epsilon_{\mathbf{k}} + \Delta_{\mathbf{k}+\mathbf{Q}} \Delta_{\mathbf{k}}}{E_{\mathbf{k}+\mathbf{Q}} E_{\mathbf{k}}} \right) \left( \frac{1}{\omega + E_{\mathbf{k}+\mathbf{Q}} + E_{\mathbf{k}} + i\eta} - \frac{1}{\omega - E_{\mathbf{k}+\mathbf{Q}} - E_{\mathbf{k}} + i\eta} \right) \quad (9)$$

We are interested in the response at large  $\mathbf{Q}$ , comparable in magnitude to  $k_F$ . In such a case, in a lattice, the current response always has a part proportional to the charge response. [6,27] This is missing in the translationally invariant model of Eq. (2).

Let us discuss the importance of the coherence factors. Note that the coherence factor contains  $-\Delta_{\mathbf{k}+\mathbf{q}} \Delta_{\mathbf{k}}$  in the charge channel, while  $+\Delta_{\mathbf{k}+\mathbf{q}} \Delta_{\mathbf{k}}$  in the spin channel. Therefore in the case of s-wave superconductors, any interesting features near Fermi-surface can arise only from the charge channel. However, d-wave superconductors have a change of sign of the gap under  $\pi/2$  rotation:

$$\Delta_{\phi} = -\Delta_{\phi+\pi/2}. \quad (10)$$

This leads to the result that the susceptibility at  $\mathbf{Q} \sim (k_F, k_F)$  from antinode(+) to antinode(-) is negligible in the charge channel, while the susceptibility at  $\mathbf{Q} \sim (2k_F, 0)$  from antinode(+) to antinode(+) is negligible in the spin channel. Therefore, the interesting features in charge channel can arise from the excitation of  $\mathbf{Q} \sim (2k_F, 0)$  and that in spin channel from the excitation of  $\mathbf{Q} \sim (k_F, k_F)$  near  $\omega = 2\Delta$ . This issue is related to the sharp magnetic neutron scattering peak which was observed in the superconducting state of  $YBa_2Cu_3O_7$  near momentum  $\mathbf{Q} = (\pi, \pi, \pi)$  ( which in our notation is  $(k_F, k_F)$  and odd with respect to inversion between the two planes per unit cell), and energy  $\omega = 41meV$ . [16–18] It was pointed out in Ref. [16] that the BCS coherence factor in neutron scattering amplitude vanishes unless  $\Delta_{\mathbf{k}}$  and  $\Delta_{\mathbf{k}+\mathbf{Q}}$  have opposite signs, because magnetic scattering is odd with respect to the time reversal symmetry. This was argued in Refs. [16,19–24] to show that the peak is a manifestation of the  $d_{x^2-y^2}$  state. Another suggestion was that the superconducting order parameter has s-wave symmetry and opposite signs in the bonding and antibonding electron bands formed with a  $Cu_2O_4$  bilayer. [25] A numerical calculation shows a collective antiferromagnetic excitation for momentum  $(\pi, \pi, \pi)$  with d-wave gap.

[26]. These calculations concentrated only on the response function in the spin channel.

We are interested in the polarizability for the momentum vectors connecting the maxima of the absolute value of the gap. Near such a maximum gap, we can expand the gap in momentum space, e.g.,

$$\begin{aligned}\Delta_{\mathbf{k}+\mathbf{Q}_0/2} &= \Delta(\cos^2 \phi - \sin^2 \phi) \\ &= \Delta \frac{(k_F + k_x)^2 - k_y^2}{(k_F + k_x)^2 + k_y^2} \approx \Delta \left(1 - 2 \frac{k_y^2}{k_F^2}\right).\end{aligned}\quad (11)$$

$\mathbf{Q}_0$  connects the (+) antinode and (+) antinode and  $\mathbf{Q}_a$  connects the (+) antinode and (-) antinode as shown in Fig. 2. The dispersion relations, e.g., Eq. (1), show that one direction of the dispersion is more slowly varying than the other; it is linear in  $k_x(k_y)$  but quadratic in  $k_y(k_x)$ . At a general  $\mathbf{Q}$ , the dispersion is linear in both  $k_x$  and  $k_y$ . A singular behavior of polarizability, if it exists, is therefore more likely for momentum near  $\mathbf{Q}_0$  and  $\mathbf{Q}_a$  at frequencies near  $2\Delta$ .

### III. S-WAVE SUPERCONDUCTORS

The long-wavelength collective modes for s-wave superconductors have been discussed earlier. [6,30,31] We concentrate on the results for large momenta. The results for the charge polarizability in this case have been already presented. [12] The details of the derivation are given in Appendix A. Near the extremum vector,  $\mathbf{Q}_0$ , in two dimensions, we found

$$\begin{aligned}\text{Re}\chi_0^{charge}(\mathbf{Q}, \omega) &\simeq -\frac{\Delta^{3/4}N_0}{E_F^{1/2}} \frac{1}{|\delta\omega|^{1/4}} \\ \text{Im}\chi_0^{charge}(\mathbf{Q}, \omega) &\simeq \begin{cases} 0 & \delta\omega < 0 \\ \frac{\pi}{2} \frac{\Delta^{3/4}N_0}{E_F^{1/2}} \frac{1}{|\delta\omega|^{1/4}} & \delta\omega > 0, \end{cases}\end{aligned}\quad (12)$$

where  $\delta\omega \equiv \omega - 2\Delta(1 + \xi^2 q^2/4)$ , and  $N_0 = v \frac{m}{2\pi}$  with  $v$ , the area of unit cell. (from now on, set  $v = 1$ .) Here,  $q$  is defined to be parallel component of  $(\mathbf{Q} - \mathbf{Q}_0)$  satisfies  $q\xi \ll 1$ , where  $\xi$  is the coherence length of the superconducting gap,  $\sim \hbar v_F/\Delta$ .

Another singularity has been also found for momentum  $\mathbf{Q}_a = (k_F, k_F)$  at energy  $2\Delta$  in agreement with earlier results(see, e.g., [25]).

$$\begin{aligned}
\text{Re}\chi_0^{charge}(\mathbf{Q}_a, \omega) &\simeq -\frac{N_0\Delta}{E_F} \ln \frac{E_F}{\sqrt{|\delta\omega|\Delta}} \\
\text{Im}\chi_0^{charge}(\mathbf{Q}_a, \omega) &\simeq \begin{cases} 0 & \delta\omega < 0 \\ \frac{\pi}{2} \frac{N_0\Delta}{E_F} & \delta\omega > 0, \end{cases} \quad (13)
\end{aligned}$$

where  $\delta\omega = \omega - 2\Delta$ .

For completeness, we also give the results for three dimensions. Singular behavior is also found in three dimensions, but it is less singular than that of two dimensions.

$$\begin{aligned}
\text{Re}\chi_0^{charge}(\mathbf{Q}_0, \omega) &\simeq -\frac{N_0\Delta}{E_F} \ln \frac{E_F}{\sqrt{|\delta\omega|\Delta}} \\
\text{Im}\chi_0^{charge}(\mathbf{Q}_0, \omega) &\simeq \begin{cases} 0 & \delta\omega < 0 \\ \frac{\pi}{2} \frac{N_0\Delta}{E_F} & \delta\omega > 0, \end{cases} \quad (14)
\end{aligned}$$

where  $N_0 = \frac{\sqrt{m^3}}{2\pi^2}$ . The singularity in the charge channel couple to phonons. Eq. (14) has been used to understand the anomalies generated in the lattice vibration spectra in the superconducting state in some compounds. [12–14] It is clear that for nested Fermi-surfaces, the polarizability become more singular. We found that the nesting along the y-direction for  $\mathbf{Q}_0$  gives  $1/\sqrt{|\omega - 2\Delta|}$  in the polarizability.

#### IV. D-WAVE SUPERCONDUCTORS

The calculation of the polarizability in d-wave superconductors is more complicated than for s-wave superconductors. Details of the calculation are given in Appendix. B. We present the results below.

We again concentrate on the case of large momentum transfers, near  $\mathbf{Q}_0$  and  $\mathbf{Q}_a$ . Referring to Fig. 2, we find that near  $\mathbf{Q}_0$ , at  $\mathbf{Q} = (2k_F - q_x, q_y)$  for  $|q_y| < \sqrt{\frac{\Delta}{E_F}}$  and  $|q_x| < (\frac{\Delta}{E_F})$ , where  $k_F = 1$ , the lowest order charge susceptibility is given by

$$\text{Re}\chi_0^{charge}(\mathbf{Q}, \omega) \simeq \begin{cases} -A \ln \left( \frac{\sqrt{8\Delta}}{\sqrt{\delta\omega - 4\Delta^3/E_F^2}} \right), & 4\frac{\Delta^3}{E_F^2} < \delta\omega \\ -B\mathbf{K}(X), & -\Delta q_y^2 - \frac{E_F^2 q_y^4}{16\Delta} < \delta\omega < 4\frac{\Delta^3}{E_F^2} \\ -B/2, & \delta\omega < -\Delta q_y^2 - \frac{E_F^2 q_y^4}{16\Delta}, \end{cases} \quad (15)$$



$$\text{Im}\chi_0^{\text{charge}}(\mathbf{Q}, \omega) \simeq \begin{cases} 0, & 4\frac{\Delta^3}{E_F^2} < \delta\omega \\ -\frac{B}{2}\ln\left(\frac{XN_0}{4B}\right), & -\Delta q_y^2 - \frac{E_F^2 q_y^4}{16\Delta} < \delta\omega < 4\frac{\Delta^3}{E_F^2} \\ -\frac{B}{2}\ln(X), & \delta\omega < -\Delta q_y^2 - \frac{E_F^2 q_y^4}{16\Delta}, \end{cases} \quad (16)$$

where

$$\begin{aligned} X &= \left( \frac{\sqrt{|1 + (E_F^2 q_y^2)/(8\Delta^2) - \sqrt{1 - \delta\omega E_F^2/(4\Delta^3)}|}}{\sqrt{1 + (E_F^2 q_y^2)/(8\Delta^2) + \sqrt{1 - \delta\omega E_F^2/(4\Delta^3)}}} \right), \\ A &= \frac{N_0}{4\sqrt{2}\sqrt{1 + (E_F^2 q_y^2)/(8\Delta^2)}}, \\ B &= \frac{N_0}{2\sqrt{2}\sqrt{1 + (E_F^2 q_y^2)/(8\Delta^2) + \sqrt{1 - \delta\omega E_F^2/(4\Delta^3)}}}, \end{aligned} \quad (17)$$

and  $\delta\omega = 2\Delta - 2\Delta q_y^2 - \omega$ .  $\mathbf{K}(X)$  is the Elliptic integral of first kind. The results above show that there is a logarithmic singularity at  $\omega = 2\Delta - 2\Delta q_y^2 - 4\Delta^3/E_F^2$  in  $\text{Re}\chi_0^{\text{charge}}$  and  $\omega = 2\Delta - \Delta q_y^2 + (E_F^2 q_y^4)/(16\Delta)$  in  $\text{Im}\chi_0^{\text{charge}}$ . The susceptibility is plotted in Fig. 3. The singularity arises just below  $2\Delta$ . The shift from  $2\Delta$ , of order  $\Delta^2/E_F^2$ , comes from the curvature of the gap. In the case of s-wave superconductor [12], the singular behavior of  $|\delta\omega|^{-1/4}$  at  $\mathbf{Q} = (2k_F, 0)$  remains at  $\omega = 2\Delta$ . For d-wave superconductors, the momentum dependence of the gap does not wipe out the singularity, but reduces it to logarithmic and changes the position of the singularity.

As explained earlier, the singularity in the polarizability in the spin channel can arise if the momentum transfer connects opposite signs of the gap. The susceptibility in the spin channel near  $\mathbf{Q}_a$ , at  $\mathbf{Q} = (k_F - q_x, k_F - q_y)$  for  $|q_x| < \frac{\Delta}{E_F}$  and  $|q_y| < \frac{\Delta}{E_F}$ , is given by

$$\begin{aligned} \text{Re}\chi_0^{\text{spin}}(\mathbf{Q}, \omega) &\simeq -\frac{N(0)\Delta}{E_F\sqrt{1+q_x^2}} \ln \frac{E_F}{\sqrt{|\delta\omega|\Delta}} \\ \text{Im}\chi_0^{\text{spin}}(\mathbf{Q}, \omega) &\simeq \begin{cases} 0 & \delta\omega < 0 \\ \frac{\pi}{2} \frac{N(0)\Delta}{E_F\sqrt{1+q_x^2}} & \delta\omega > 0, \end{cases} \end{aligned} \quad (18)$$

where  $\delta\omega = 2\Delta - 2\Delta q_x^2 - 8\Delta^3 q_x^2/E_F^2 - \omega$ .

As we see, there is also a logarithmic singularity in the spin channel. But it is important to note that the amplitude of the singularity of the charge channel is bigger than that of the spin channel by the  $O(E_F/\Delta)$ .

### A. Susceptibility in the Random Phase Approximation

The next step is to see how the lowest order polarizability is modified due to the interactions among the quasiparticles. We present the approximate renormalized polarizability in the present section. In the random phase approximation,

$$\chi = \frac{\chi_0}{1 + V\chi_0} \quad (19)$$

where we assume that the interaction  $V_Q = -V$ . This has a singular part in charge channel with a pole at frequency  $\omega_Q$  with weight  $r_Q$  and a regular part which is approximately a constant for  $\omega > 1.5\Delta$ . The position of the pole,  $\omega_Q$ , in  $\chi$  is given by

$$\begin{aligned} \omega_Q &= 2\Delta - 2\Delta q_y^2 - 4\Delta^3/E_F^2 - 8\Delta e^{-\frac{1}{AV}} \\ &= 2\Delta - 2\Delta q_y^2 - 4\Delta^3/E_F^2 - 8\Delta e^{-\frac{\sqrt{8+(E_F^2 q_y^2)/\Delta^2}}{N_0 V}}. \end{aligned} \quad (20)$$

The weight of the pole is

$$\begin{aligned} r_Q &= \frac{8\Delta}{AV^2} e^{-\frac{1}{AV}} \\ &= \frac{16\sqrt{2}\Delta\sqrt{1+(E_F^2 q_y^2)/(8\Delta^2)}}{N_0 V^2} e^{-\frac{\sqrt{8+(E_F^2 q_y^2)/\Delta^2}}{N_0 V}}. \end{aligned} \quad (21)$$

Four parameters,  $N_0V$ ,  $\Delta/E_F$ ,  $\Delta/V$ , and  $q_y$  determine the position and the strength of the poles. Let us fix  $N_0V \sim 1$  and  $\Delta/E_F \sim \Delta/V \sim 0.1$ . At  $q_y = 0$ , the position of pole is at  $\omega = 1.49\Delta$  and the weight is  $r = 0.13$ . At  $q_y = 0.2$ , the position of pole is at  $\omega = 1.62\Delta$  and the weight is  $r = 0.087$ . For the reasonable condition  $|q_y| < \sqrt{\Delta/E_F} \sim 0.3$ , the pole is at about  $\omega_0 = 1.5\Delta$  and the weight is  $\sim 0.1$ .

### B. Polarizability with a marginal Fermi-liquid vertex

The anomalous normal state transport properties near the doping for maximum  $T_c$  can be understood through a phenomenological scale-invariant particle-hole spectrum, (Eq. (22), see below) which at frequencies large compared to temperature is a constant, independent of momentum(except in the hydrodynamic regime) and of frequency up to a cut-off  $\nu_c$ .

$$\text{Im}\chi_{MFL}(q, \nu) \approx N(0); \quad T \ll \nu < \nu_c, \quad (22)$$

The polarizability can in general be represented as in Fig. 4. If we take for  $\Gamma$  a phenomenological, momentum independent vertex whose imaginary part is  $\approx iN(0)^{-1}$  for  $T \ll \nu < \nu_c$ ,

$$\chi_{MFL}(q, \nu) = \Gamma(\nu) \left( \sum_{k, \omega} \Lambda_{k, q} G(k + q, \omega + \nu) G(k, \omega) \right)^2, \quad (23)$$

Eq. (22) is then essentially reproduced. Here  $G$  is the normal state Green's function and  $\Lambda$ 's are appropriate vertices. In the preceding section, we put  $\Gamma \sim \delta_{q, q'} \delta_{\omega, \omega'}$  in Fig. 4. This leads to major difference between  $\chi_{MFL}$  in the normal state and  $\chi_0$  of Eqs. (4) and (5). But for the superconducting state, the results are qualitatively similar if we make the further assumption that  $\Gamma(\nu)$  does not change in the passage to the superconducting state. This assumption is almost certainly incorrect. But as long as  $\Gamma(\nu)$  does not develop any sharp features for energies below  $2\Delta$  in the superconducting state, the results are unlikely to be qualitatively altered. This is because of the sharp drop in  $\chi_0$  for energies below  $2\Delta$  which we have calculated. Using (15) in (23), we see that the *log* singularities near  $2\Delta$  change to *log*<sup>2</sup>( $\dots$ ) singularities. Within the approximation of the phenomenology this difference is not important. There is one important difference however,  $\chi$  in Fig. 3 and in Eq. (23) is the total polarizability, not the reducible polarizability. So no further manipulation as in section (A) is now not permitted.

### C. Single particle spectral function in the superconducting state

The singularity in the polarizability at large momentum provides important modification in the single particle spectra. The singular contribution to the polarizability in the spin channel and in the current channel for translationally invariant case is  $O(\Delta/E_F)$  smaller than the charge channel. As we already mentioned, in a lattice the polarizability in the current channel is proportional (and usually of similar magnitude) to the charge channel. We may therefore ignore the spin channel.

Generalized self energy can be obtained using the diagram shown in Fig. 5. [15]

$$\begin{aligned}
\Sigma(k) &= i \int \frac{d^3q}{(2\pi)^3} (V\tau_3)\psi_{k-q}^\dagger \chi(q)\psi_{k-q}(V\tau_3) \\
&= i \int \frac{d^3q}{(2\pi)^3} V^2\tau_3 G(k-q)\chi(q)\tau_3
\end{aligned} \tag{24}$$

where  $k = (\mathbf{k}, \omega)$ . Here we neglect the other self energy contribution shown in Fig. 5(c) ;

$$-i \int \frac{d^3q}{(2\pi)^3} V^2\tau_3 \text{Tr}[\tau_3 G(k-q)] \tag{25}$$

It is clear that this is negligible because it is of the order of  $O(\epsilon_{\mathbf{k}}/E_{\mathbf{k}})$  and we are near the Fermi-surface.

We write  $\chi(\mathbf{Q}, \omega)$  as the sum of a singular part and a regular part.

$$\chi(\mathbf{Q}, \omega) \approx \frac{2\omega_Q r_Q}{\omega^2 - \omega_Q^2 + i\eta} f(Q) + \chi_{reg}. \tag{26}$$

We will define  $\Sigma^{sing}$  as the contribution of the first part and  $\Sigma^{reg}$  as the second one with

$$\Sigma(\omega, \mathbf{k}) = \Sigma^{sing}(\omega, \mathbf{k}) + \Sigma^{reg}(\omega, \mathbf{k}). \tag{27}$$

For a d-wave superconductors  $f(Q)$  gives the momentum limits shown as above,  $\mathbf{Q} = (2k_F - q_x, q_y)$  where  $|q_x| < \Delta/E_F$  and  $|q_y| < \sqrt{\Delta/E_F}$  setting  $k_F = 1$ . We assume that  $\omega_Q = \omega_0$ , and  $r_Q = r$  in this range.

The self energy,  $\Sigma^{sing}(\omega, \mathbf{k})$  in the charge channel is

$$\begin{aligned}
\Sigma^{sing}(\omega, \mathbf{k}) &= i \int \frac{d\omega_1 d^2Q}{(2\pi)^2} (V\tau_3) G_0(\omega + \omega_1, \mathbf{k} + \mathbf{Q})(V\tau_3)\chi(\omega_1, \mathbf{Q}) \\
&= i \int \frac{d\omega_1 d^2Q}{(2\pi)^2} (V\tau_3) \frac{(\omega + \omega_1)I + \epsilon_{\mathbf{k}+\mathbf{Q}}\tau_3 + \Delta_{\mathbf{k}+\mathbf{Q}}\tau_1}{(\omega + \omega_1)^2 - E_{\mathbf{k}+\mathbf{Q}}^2 + i\eta} (V\tau_3) \frac{2\omega_0 r}{\omega_1^2 - \omega_0^2 + i\eta}.
\end{aligned} \tag{28}$$

After performing the frequency intergral, we found that the singular part of the self energy is given by

$$\begin{aligned}
\Sigma_I(\omega, \mathbf{k}) &= V^2 r \int \frac{d^2Q}{8\pi^2} \left( \frac{1}{2} \right) \left( \frac{1}{\omega + \omega_0 + E_{\mathbf{k}+\mathbf{Q}} + i\eta} \right. \\
&\quad \left. + \frac{1}{\omega - \omega_0 - E_{\mathbf{k}+\mathbf{Q}} + i\eta} \right)
\end{aligned} \tag{29}$$

$$\begin{aligned}
\Sigma_{\tau_1}(\omega, \mathbf{k}) &= V^2 r \int \frac{d^2Q}{8\pi^2} \left( \frac{\Delta_{\mathbf{k}+\mathbf{Q}}}{2E_{\mathbf{k}+\mathbf{Q}}} \right) \left( \frac{1}{\omega + \omega_0 + E_{\mathbf{k}+\mathbf{Q}} + i\eta} \right. \\
&\quad \left. - \frac{1}{\omega - \omega_0 - E_{\mathbf{k}+\mathbf{Q}} + i\eta} \right),
\end{aligned} \tag{30}$$

$$\Sigma_{\tau_3}(\omega, \mathbf{k}) = -V^2 r \int \frac{d^2 Q}{8\pi^2} \left( \frac{\epsilon_{\mathbf{k}+\mathbf{Q}}}{E_{\mathbf{k}+\mathbf{Q}}} \right) \left( \frac{1}{\omega + \omega_0 + E_{\mathbf{k}+\mathbf{Q}} + i\eta} + \frac{1}{\omega - \omega_0 - E_{\mathbf{k}+\mathbf{Q}} + i\eta} \right). \quad (31)$$

After expanding  $E_{\mathbf{k}+\mathbf{Q}}$  near maximum gap(+), we obtained the self energy for  $k_x \sim -k_F + k'_x$  where  $|k'_x| < |q_x|$  and  $|k_y| < |q_y|$ ,

$$\begin{aligned} \text{Re}\Sigma_I(\omega, \mathbf{k}) &= \frac{V^2 N_0 r}{4\sqrt{2}} \left[ \arcsin \frac{2\Delta}{\sqrt{E_F(\omega^* - \omega)}} \theta\left(-\omega + \omega^* - \frac{4\Delta^2}{E_F}\right) \right. \\ &\quad \left. - \arcsin \frac{2\Delta}{\sqrt{E_F(\omega^* + \omega)}} \theta\left(\omega + \omega^* - \frac{4\Delta^2}{E_F}\right) \right] \\ \text{Im}\Sigma_I(\omega, \mathbf{k}) &= \frac{V^2 N_0 r}{4\sqrt{2}} \left[ -\text{arcsinh} \frac{2\Delta}{\sqrt{E_F(-\omega^* + \omega)}} \theta(\omega - \omega^*) \right. \\ &\quad \left. + \text{arcsinh} \frac{2\Delta}{\sqrt{E_F(-\omega^* - \omega)}} \theta(-\omega - \omega^*) \right] \end{aligned} \quad (32)$$

$$\begin{aligned} \text{Re}\Sigma_{\tau_1}(\omega, \mathbf{k}) &= -\frac{V^2 N_0 r}{4\sqrt{2}} \left[ \arcsin \frac{2\Delta}{\sqrt{E_F(\omega^* - \omega)}} \theta\left(-\omega + \omega^* - \frac{4\Delta^2}{E_F}\right) \right. \\ &\quad \left. + \arcsin \frac{2\Delta}{\sqrt{E_F(\omega^* + \omega)}} \theta\left(\omega + \omega^* - \frac{4\Delta^2}{E_F}\right) \right] \\ \text{Im}\Sigma_{\tau_1}(\omega, \mathbf{k}) &= \frac{V^2 N_0 r}{4\sqrt{2}} \left[ \text{arcsinh} \frac{2\Delta}{\sqrt{E_F(-\omega^* + \omega)}} \theta(\omega - \omega^*) \right. \\ &\quad \left. + \text{arcsinh} \frac{2\Delta}{\sqrt{E_F(-\omega^* - \omega)}} \theta(-\omega - \omega^*) \right], \end{aligned} \quad (33)$$

where  $\omega^* = \omega_0 + \Delta - 4\Delta k_y^2 + E_F^2/\Delta(k_y^2 - 2k'_x)^2$ .  $\Sigma_{\tau_3}$  is basically the same as  $\epsilon_k/\Delta_k \Sigma_{\tau_1}$ , expanding the  $\epsilon_{\mathbf{k}+\mathbf{Q}} = -\epsilon_{\mathbf{k}} + O(\mathbf{q})$  with  $E_{\mathbf{k}+\mathbf{Q}} = E_{\mathbf{k}}$ .

We now discuss  $\chi_{reg}$ . This depends on whether one uses the form Eqs. (15) and (16) for  $\chi_0$  or the marginal form. This difference is important for large frequencies, because the single particle spectra for the former case reverts to the Fermi liquid form, which disagrees with experiments. So we consider the marginal fermi-liquid form. An important issue in that case is the form of  $\chi_{reg}$  for low frequencies in the d-wave superconductor. In a d-wave superconductor, the regular part of  $\chi_{reg}(\mathbf{Q}, \nu)$  at low energies is dominated by the particle-hole excitations with  $\mathbf{Q}$  connecting the nodes of the gap function  $\Delta_{\mathbf{k}}$ . These determine the

lifetime of low energy quasiparticles and the low temperature thermodynamics. But they are not involved in the scattering of quasiparticles near the maximum of the gap due to restrictions of momentum conservation. For the relaxation of such quasiparticles, we may therefore assume a marginal Fermi-liquid form for energies above  $2\Delta$ :

$$\chi_{reg}(\mathbf{Q}, \nu) = r_{reg}(\mathbf{Q})N_0\theta(\nu - 2\Delta), \quad \nu < \nu_c, \quad (34)$$

with  $r_{reg} + r = 1$ . This produces

$$\text{Im}\Sigma_{I(\tau_1)}^{reg} \propto \mp|\omega|\theta(\omega - 3\Delta) + |\omega|\theta(-\omega - 3\Delta). \quad (35)$$

Fig. 6 shows the Re and Im parts of self-energy for excitations near the maximum gap including both the singular and the regular parts of the fluctuations.

The one particle Green's function can be obtained using

$$\begin{aligned} G^{-1} &= G_0^{-1} - \Sigma \\ &= \begin{pmatrix} \omega - \epsilon_{\mathbf{k}} + \Sigma_{\tau_3} - \Sigma_I & -\Delta_{\mathbf{k}} - \Sigma_{\tau_1} \\ -\Delta_{\mathbf{k}} - \Sigma_{\tau_1} & \omega + \epsilon_{\mathbf{k}} - \Sigma_{\tau_3} - \Sigma_I \end{pmatrix} \end{aligned} \quad (36)$$

The spectral function is give by:

$$\begin{aligned} A(\omega, \mathbf{k}) &= \frac{-sgn(\omega)}{\pi} \text{Im}G_{11} \\ &= \frac{-sgn(\omega)}{\pi} \text{Im} \frac{\omega - \epsilon_{\mathbf{k}} + \Sigma_{\tau_3} - \Sigma_I}{(\omega - \epsilon_{\mathbf{k}} + \Sigma_{\tau_3} - \Sigma_I)(\omega + \epsilon_{\mathbf{k}} - \Sigma_{\tau_3} - \Sigma_I) - (\Delta_{\mathbf{k}} + \Sigma_{\tau_1})^2 + i\eta}. \end{aligned} \quad (37)$$

The spectral function is plotted in Fig. 7 for  $\mathbf{k}$  near the maximum point of the gap and for the representative values,  $V \sim E_F = 10\Delta$ . For  $0 < \omega < 2\Delta$  where  $\text{Im}\Sigma_I = \text{Im}\Sigma_{\tau_1} = 0$ , it is a delta function near  $\omega \sim \Delta$  and has a broad hump at  $\omega \sim 2.5\Delta$ . As we change  $\mathbf{k}$ , we find the peak near  $\Delta$  shifts slower than the change of  $\epsilon_{\mathbf{k}}$ , itself. The position of the broad hump shifts by  $\Delta k_y^2$  which can be up to order of  $\Delta^2/E_F$ . The broad peak would become smooth if the contributions from the other excitations, e.g., node-node excitations are included. The excitations from node to node contribute to finite life time of quasiparticle for  $\omega > \Delta$  which are not included here. However, this would not change the qualitative behavior of the broad peak.

## V. DISCUSSION

We have found a new collective mode for large momentum at energy just below  $2\Delta$ , which can be detected by inelastic x-ray scattering or electron scattering. Since neutrons have a negligible cross-section for scattering with electronic density fluctuations, this mode cannot be detected by neutron scattering. The calculations, done using an isotropic Fermi-surface give a lower limit to the spectral weight of the collective modes. Realistic band-structures show some nesting in the region of the maximum gap due to which stronger effects are to be expected in experiments.

We have also calculated the single particle spectral function which is strongly affected for states near the maximum of the gap by the collective mode. This quantity has been measured by ARPES [11]. ARPES on *Bi2212* near  $(\pi, 0)$  in the superconducting state shows two features. There exists a sharp peak around  $40\text{meV}$  and a broad hump at about  $100\text{meV}$ . Our results also show two peaks in the spectral function, a sharp peak near  $\Delta$  and a broad peak near  $2.5\Delta$ . When we change the momentum by  $\mathbf{k}$  in a direction perpendicular to the Fermi-surface from the point of gap-maximum, the sharp peak and the broad peak shift as  $E_F k'_x$  where  $k'_x$  can vary up to  $\Delta/E_F$  (See Fig. 7 (d), and Fig. 2 (c) in Ref. [11]). For a change of momentum transverse to the Fermi-surface, this variation is cancelled to leading order by a similar decrease in the value of the gap. (See Fig. 7 (b), (c), and Fig. 2 (b) in Ref. [11]) These features are generally consistent with the experiments, although the persistence of the sharp feature near  $\Delta$  is over a wider region than calculated by us. We think this is probably due to the nesting and Van-Hove dispersions of the band-structure near the points of gap-maximum.

It is also apparent in the experiments that when the sharp peak disappears, the broad peak start to move rapidly as in the normal state. This is also consistent with our expectation that the behavior of spectral function must be similar to that of normal state for  $\epsilon_{\mathbf{k}}$  away from the chemical potential by much more than  $\Delta$ .

We, finally, mention the limitation of our results. Due to the use of an isotropic Fermi-

surface, the range of momentum where our results are valid is rather limited. Another limitation of our results is that the one particle Green function  $G$  is not calculated self-consistently. We start with  $G$  of the BCS form. The singular self energy corrections split the BCS peak in the spectral function into two peaks. But we do not go back and calculate the particle-hole fluctuations and the self-energy with the renormalized  $G$ . We expect that using renormalized particle  $G$ , additional features at higher energy( near  $5\Delta$ ) appears and the features already calculated are sharpened. The magnitude of these higher order effects is expected to be of order  $N(0)V\Delta/E_F$ . We have not included the vertex corrections in a systematic fashion either but have contented ourselves with a phenomenological requirement that the vertex be such that the spectral function in the superconducting state reverts to that of the normal state at large enough energy. Another limitation is the assumption of the sharp change as a function of  $\nu$  in Eq. (34). We expect a rapidly varying but smooth function. This would tend to broaden the onset of the hump in the spectral functions in Fig. 7.

### APPENDIX A:

We show how to evaluate the integrals to obtain the results quoted in Ref. [12] and section III of this paper. After performing the frequency integral in Eq. (4), one must evaluate

$$\int d^d k \frac{E_{\mathbf{k}} E_{\mathbf{k}+\mathbf{Q}} - \epsilon_{\mathbf{k}} \epsilon_{\mathbf{k}+\mathbf{Q}} + \Delta^2}{E_{\mathbf{k}} E_{\mathbf{k}+\mathbf{Q}}} \left( \frac{1}{E_{\mathbf{k}} + E_{\mathbf{k}+\mathbf{Q}} - \omega + i\eta} + \frac{1}{E_{\mathbf{k}} + E_{\mathbf{k}+\mathbf{Q}} + \omega - i\eta} \right) \quad (\text{A1})$$

The coherence factor does not play an important role for large  $\mathbf{Q}$  so that we simply put it  $O(1)$ . Both  $E_{\mathbf{k}}$  and  $E_{\mathbf{k}+\mathbf{Q}}$  are bounded from below by  $\Delta$ . Now expand  $E_{\mathbf{k}}$  and  $E_{\mathbf{k}+\mathbf{Q}}$  near the chemical potential in cartesian coordinates and (without loss of generality) take  $\mathbf{Q}$  along  $x$ -axis. First consider  $\mathbf{Q}_0 = 2k_F \hat{x}$ ,

$$\epsilon_{\mathbf{k}} = -v_F p_x + \frac{p_y^2}{2m} + \frac{p_z^2}{2m} + O(p_x^2) \quad (\text{A2})$$



where  $p_x = (k_x - k_{Fx})$ ,  $p_y = (k_y - k_{Fy})$  and  $p_z = (k_z - k_{Fz})$ ,  $p$ 's are  $\ll k_F$ 's, where  $k_F = (k_{Fx}, k_{Fy}, k_{Fz})$ . (For this  $\mathbf{Q}_0$ ,  $k_{Fy} = k_{Fz} = 0$ )

$$\epsilon_{\mathbf{k}+\mathbf{Q}_0} = v_F p_x + \frac{p_y^2}{2m} + \frac{p_z^2}{2m} + O(p_x^2) \quad (\text{A3})$$

Now  $E_{\mathbf{k}}$  and  $E_{\mathbf{k}+\mathbf{Q}}$  can be expand as follows.

$$\begin{aligned} E_{\mathbf{k}} &= \Delta + \frac{\epsilon_{\mathbf{k}}^2}{2\Delta} \\ E_{\mathbf{k}+\mathbf{Q}_0} &= \Delta + \frac{\epsilon_{\mathbf{k}+\mathbf{Q}_0}^2}{2\Delta} \end{aligned} \quad (\text{A4})$$

The integral of Eq. (A1) becomes

$$\int_0^\infty d^d p \frac{1}{(2\Delta - \omega) + \frac{1}{\Delta} [v_F^2 p_x^2 + (p_y^2/2m + p_z^2/2m)^2]} \quad (\text{A5})$$

One can see immediately by power counting, for three dimensions, we have  $\log|\omega - 2\Delta|$  singularity as  $\mathbf{p}$  approaches 0 (means  $\mathbf{k} \rightarrow \mathbf{k}_F$ ). For two dimensions, we have  $[\omega - 2\Delta]^{-1/4}$  singularity.

For general  $\mathbf{Q}$ , again choose  $\mathbf{Q}$  parallel to  $x$ -axis without loss of any generality and define  $\mathbf{Q} = 2Q_x \hat{x} = 2k_{Fx} \hat{x}$  (See Fig. A2). We again expand in terms of the  $p$ 's defined above.

$$\begin{aligned} \epsilon_{\mathbf{k}} &= -\frac{Q_x}{m} p_x + \frac{k_{Fy}}{m} p_y + \frac{k_{Fz}}{m} p_z + \frac{p_x^2}{2m} + \frac{p_y^2}{2m} + \frac{p_z^2}{2m} \\ \epsilon_{\mathbf{k}+\mathbf{Q}} &= \frac{Q_x}{m} p_x + \frac{k_{Fy}}{m} p_y + \frac{k_{Fz}}{m} p_z + \frac{p_x^2}{2m} + \frac{p_y^2}{2m} + \frac{p_z^2}{2m} \end{aligned} \quad (\text{A6})$$

Unlike Eqs. (A2) and (A3), linear terms in  $p_y$  and  $p_z$  are present in Eq. (A6). This changes the power counting. When we do the same expansion as in Eq. (A4) and do the integral, we see by just power counting that in the lowest order of polarizability the  $\log$  is cut off by the  $k_{Fy}^2/2m$  and  $k_{Fz}^2/2m$  terms in three dimensions. (In fact, it has  $\log$  singularity in two dimensions with coefficient depending on  $\mathbf{Q}$  and changing to the stronger singularity mentioned above at  $\mathbf{Q}_0 = 2k_F \hat{x}$ )

To summarize, singularity at  $\omega = 2\Delta$  for  $d = 3$  is found for only  $\mathbf{Q}_0 = 2k_F \hat{x}$  (or  $\ll \xi^{-1}$ ) where the leading terms of  $p_x$  is linear and  $p_y, p_z$  are quadratic in Eq. (A6).

## APPENDIX B:

We show here how to evaluate the integrals to get the results quoted in section IV. We start with Eq. (7) in section II. Expand  $\epsilon_{\mathbf{k}}$  near the Fermi-surface and  $\Delta_{\mathbf{k}}$  near the maximum gap(See Eq. (2) and (11) in section II). For  $\mathbf{k} = (-k_F + p_x, p_y)$

$$E_{\mathbf{k}} \simeq \Delta - 2\Delta p_y^2 + \frac{E_F^2}{\Delta}(2p_x^2 - 2p_x p_y^2 + p_y^4/2), \quad (\text{B1})$$

where  $E_F = k_F^2/(2m)$  and  $p_{x(y)} \equiv p_{x(y)}/k_F$  (we set  $k_F = 1$ ). Note that it contains  $2\Delta p_y^2$  term due to the anisotropy of the gap. We can also find  $E_{\mathbf{k}+\mathbf{Q}_0}$  near  $\mathbf{Q}_0$ ;  $(k_x, k_y) = (k_F - q_x + p_x, p_y + q_y)$ . The expression for  $E_{\mathbf{k}} + E_{\mathbf{k}+\mathbf{Q}_0} - \omega$  is written as follows.

$$\begin{aligned} f(p_x, p_y) &= E_{\mathbf{k}} + E_{\mathbf{k}+\mathbf{Q}_0} - \omega \\ &= \frac{E_F^2}{\Delta}(4p_x^2 + 4p_x q_y p_y + 2q_y^2 p_y^2 + 2q_y p_y^3 + p_y^4) - 4\Delta q_y p_y - 4\Delta p_y^2 + 2\Delta - 2\Delta q_y^2 - \omega. \end{aligned} \quad (\text{B2})$$

The susceptibility is obtained by integrating the  $1/f(p_x, p_y)$  with respect to  $p_x$  and  $p_y$ . After integrating over  $p_x$  ( $-\Delta/E_F < p_x < \Delta/E_F$ ) we have

$$\begin{aligned} \int \frac{1}{f(p_x, p_y)} dp_x &= \frac{\Delta}{E_F^2} \frac{1}{\sqrt{(p_y^2 + q_y p_y - \frac{2\Delta^2}{E_F^2})^2 + \frac{\delta\omega\Delta}{E_F^2} - \frac{4\Delta^4}{E_F^4}}} \\ &\quad \times \arctan \frac{q_y p_y + 2}{\sqrt{(p_y^2 + q_y p_y - \frac{2\Delta^2}{E_F^2})^2 + \frac{\delta\omega\Delta}{E_F^2} - \frac{4\Delta^4}{E_F^4}}} \end{aligned} \quad (\text{B3})$$

The leading term of this function is

$$\frac{\pi}{2} \frac{\Delta}{E_F^2} \frac{1}{\sqrt{(p_y^2 + q_y p_y - \frac{2\Delta^2}{E_F^2})^2 + \frac{\delta\omega\Delta}{E_F^2} - \frac{4\Delta^4}{E_F^4}}} \quad (\text{B4})$$

After performing the intergration over  $p_y$ , we have the Elliptical function.

$$K(k) = \int_0^1 \frac{dx}{\sqrt{(1-x^2)(1-k^2x^2)}}, \quad (\text{B5})$$

where

$$k = \left( \frac{\sqrt{1 + (E_F^2 q_y^2)/(8\Delta^2) - \sqrt{1 - \delta\omega E_F^2/(4\Delta^3)}}}{\sqrt{1 + (E_F^2 q_y^2)/(8\Delta^2) + \sqrt{1 - \delta\omega E_F^2/(4\Delta^3)}}} \right). \quad (\text{B6})$$

When two poles of Elliptical function coincide(  $k = 1$ ), we have a *log* singularity, which happens here at  $\delta\omega = 4\Delta^3/E_F^2$ .

$$\begin{aligned}\text{Re}\chi_0(\mathbf{Q}_0, \omega) &= -\frac{1}{4\pi^2} \int \frac{1}{f(p_x, p_y)} dp_x dp_y \\ &= -\frac{N_0}{\sqrt{8 + (E_F^2 q_y^2)/\Delta^2}} \ln \left( \frac{8\Delta}{|\delta\omega - 4\Delta^3/E_F^2|} \right),\end{aligned}\quad (\text{B7})$$

where  $N_0 = 1/(4\pi E_F)$ .

The singular part of self-energy for spin-spin correlation function is also presented here which are similar to those of the charge channel apart from signs.

$$\begin{aligned}\text{Re}\Sigma_I &= \frac{V^2 N_0 r}{2\sqrt{2}} \left[ \arcsin \frac{2\Delta}{\sqrt{E_F(3\Delta - \omega)}} \theta\left(-\omega + 3\Delta - \frac{4\Delta^2}{E_F}\right) \right. \\ &\quad \left. - \arcsin \frac{2\Delta}{\sqrt{E_F(3\Delta + \omega)}} \theta\left(\omega + 3\Delta - \frac{4\Delta^2}{E_F}\right) \right] \\ \text{Im}\Sigma_I &= \frac{V^2 N_0 r}{4\sqrt{2}} \left[ -\text{arcsinh} \frac{2\Delta}{\sqrt{E_F(-3\Delta + \omega)}} \theta(\omega - 3\Delta) \right. \\ &\quad \left. + \text{arcsinh} \frac{2\Delta}{\sqrt{E_F(-3\Delta - \omega)}} \theta(-\omega - 3\Delta) \right]\end{aligned}\quad (\text{B8})$$

$$\begin{aligned}\text{Re}\Sigma_{\tau_1} &= \frac{V^2 N_0 r}{2\sqrt{2}} \left[ \arcsin \frac{2\Delta}{\sqrt{E_F(3\Delta - \omega)}} \theta\left(-\omega + 3\Delta - \frac{4\Delta^2}{E_F}\right) \right. \\ &\quad \left. + \arcsin \frac{2\Delta}{\sqrt{E_F(3\Delta + \omega)}} \theta\left(\omega + 3\Delta - \frac{4\Delta^2}{E_F}\right) \right] \\ \text{Im}\Sigma_{\tau_1} &= -\frac{V^2 N_0 r}{4\sqrt{2}} \left[ \text{arcsinh} \frac{2\Delta}{\sqrt{E_F(-3\Delta + \omega)}} \theta(\omega - 3\Delta) \right. \\ &\quad \left. + \text{arcsinh} \frac{2\Delta}{\sqrt{E_F(-3\Delta - \omega)}} \theta(-\omega - 3\Delta) \right]\end{aligned}\quad (\text{B9})$$

Note that the weight,  $r$ , here is smaller than that in Eqs. (32) and (33) by order of  $\Delta/E_F$ .

## REFERENCES

- [1] See e.g., W. N. Hardy, *et al.*, Phys. Rev. Lett. **70**, 3999 (1993); K. A. Moler, *et al.*, Phys. Rev. Lett. **73**, 2744 (1994); A. Maeda, *et al.*, Phys. Rev. Lett. **74**, 1202(1995); C. C. Tsuei, *et al.*, Phys. Rev. Lett. **73**, 593 (1994); D. A. Wollman, *et al.*, Phys. Rev. Lett. **74**, 797 (1995).
- [2] C. M. Varma *et al.*, Phys. Rev. Lett. **63**, 1996 (1989).
- [3] C. G. Olson *et al.*, Science **245**, 731 (1989); Phys. Rev. B **42**, 381 (1990).
- [4] Y. Kuroda and C. M. Varma, Phys. Rev. B **42**, 8619 (1990).
- [5] M. C. Nuss *et al.*, Phys. Rev. Lett. **66**, 3305 (1991)
- [6] P. B. Littlewood and C. M. Varma, Phys. Rev. B **46**, 405 (1992).
- [7] Z. X. Shen and D. S. Dessau, Phys. Rep. **253**, 1 (1995).
- [8] H. Ding *et al.*, Phys. Rec. Lett. **76**, 1533 (1996).
- [9] J. C. Campuzano *et al.*, Phys. Rev. B **53**, R14737 (1996).
- [10] H. Ding *et al.*, Phys. Rev. Lett. **78**, 2628 (1997)
- [11] M. R. Norman *et al.*, Phys. Rev. Lett. **79**, 3506 (1997)
- [12] Hae-Young Kee and C. M. Varma, Phys. Rev. Lett. **79** 4250, (1997).
- [13] H. Kawano *et al.*, Phys. Rev. Lett. **77**, 4628 (1996).
- [14] C. Stassis *et al.*, Phys. Rev. B **55**, R8678 (1997).
- [15] J. R. Schrieffer, *Theory of Superconductivity* (Benjamin/Cummings, Reading, Massachusetts, 1964).
- [16] H. F. Fong *et al.*, Phys. Rev. Lett. **75**, 316 (1995).
- [17] J. Rossat-Mignod *et al.*, Physica (Amsterdam) **185-189C**, 86 (1991).

- [18] H. A. Mook *et al.*, Phys. Rev. Lett. **70**, 3490 (1993)
- [19] N. Bulut and D.J. Scalapino, Phys. Rev. B **47**, 3419 (1993).
- [20] P. Monthoux and D.J. Scalapino, Phys. Rev. Lett. **72**, 1874 (1994).
- [21] K. Maki and H. Won, Phys. Rev. Lett. **72**, 1758 (1994); H. Won and K. Maki, Phys. Rev. B **49**, 15305 (1994).
- [22] G. Stemmann, C. Pepin, and M. Lavagna, Phys. Rev. B **50**, 4075 (1994).
- [23] M. Lavagna and G. Stemmann, Phys. Rev. B **49**, 4235 (1994).
- [24] F. Onufreieva and J. Rossat-Mignod, Phys. Rev. B **52**, 7572 (1995).
- [25] I. I. Mazin and V. M. Yakovenko, Phys. Rev. Lett. **75**, 4134 (1995).
- [26] N. Bulut and D. J. Scalapino, Phys. Rev. B **53**, 5149 (1996).
- [27] A. A. Abrikosov and V. M. Genkin, JEPT **38**, 417 (1974).
- [28] W. Kohn, Phys. Rev. Lett. **2**, 393 (1959).
- [29] M. E. Flatté, Phys. Rev. B. **50**, 1190 (1994).
- [30] P. W. Anderson, Phys. Rev. **110**, 827 (1958); **112**, 1900 (1958); N. N. Bogoliubov, Nuovo Cimento **7**, 794 (1958).
- [31] Y. Nambu and G. Jona-Lasinio, Phys. Rev. **122**, 345 (1961).
- [32] M. R. Norman and H. Ding, preprint.
- [33] J. P. Lu, Phys. Rev. Lett. **68**, 125 (1992).

## FIGURES

FIG. 1. The isotropic Fermi-surface with radius  $k_F$  illustrating the vectors,  $\mathbf{Q}_0 = (2k_F, 0)$  and  $\mathbf{Q}_a = (k_F, k_F)$ , used in the text.

FIG. 2. The isotropic Fermi-surface with d-wave gap symmetry illustrating vectors defined in the text. The (+) and (-) denote the the signs of the gap.  $\mathbf{Q}_0$  and  $\mathbf{Q}_a$  are momentum transfer between two maximum gaps with same and different signs, respectively. The range of  $q_x$  and  $q_y$  where our results for the polarizabilities are valid are shown as shaded ellipse.

FIG. 3. (a) The imaginary part of the lowest order polarizability,  $\text{Im}\chi_0^{charge}(\mathbf{Q}_0, \omega)$ . (b) The real part of the lowest order polarizability,  $\text{Re}\chi_0^{charge}(\mathbf{Q}_0, \omega)$ . The parameters are the same as those in the text;  $N_0V \sim 1$  and  $\Delta/E_F \sim \Delta/V \sim 0.1$ .

FIG. 4. The diagrammatic representation of the polarizability with vertices  $\Lambda$  and  $\Gamma(\nu)$ .

FIG. 5. (a) The renormalized interaction after RPA. (b) The lowest order self-energy; exchange contribution from the Coulomb interaction (c) The lowest order self-energy; direct contribution from the Coulomb interaction.

FIG. 6. The lowest order self energy. (a)  $\text{Re}\Sigma_I(\omega, \mathbf{k})$ , (b)  $\text{Im}\Sigma_I(\omega, \mathbf{k})$ , (c)  $\text{Re}\Sigma_{\tau_1}(\omega, \mathbf{k})$ , and (d)  $\text{Im}\Sigma_{\tau_1}(\omega, \mathbf{k})$ , where  $\mathbf{k}$  is near the maximum gap. The parameters are the same as those in the text;  $N_0V \sim 1$ ,  $\Delta/E_F \sim \Delta/V \sim 0.1$ , and  $r \sim 0.1$

FIG. 7. The spectral function  $A(\omega, \mathbf{k})$  with (a)  $\mathbf{k} = (-k_F, 0)$ , (b)  $\mathbf{k} = (-k_F, 0.1k_F)$ , (c)  $\mathbf{k} = (-k_F, 0.2k_F)$ , and (d)  $\mathbf{k} = (-1.05k_F, 0)$ . The parameters are the same as those in the text;  $N_0V \sim 1$ ,  $\Delta/E_F \sim \Delta/V \sim 0.1$ ,  $r \sim 0.1$ , and  $r_{reg} \sim 0.9$

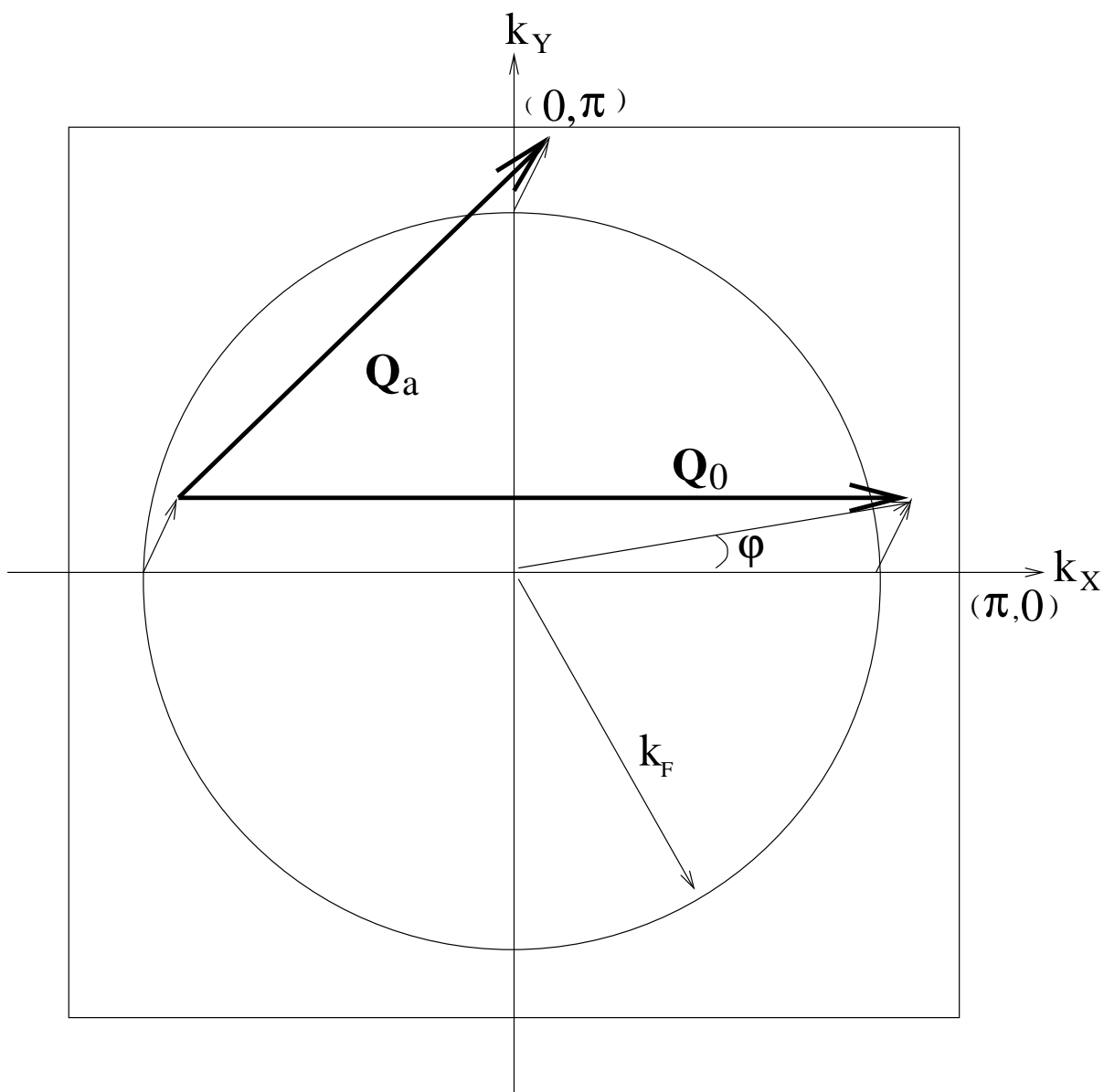


Fig. 1

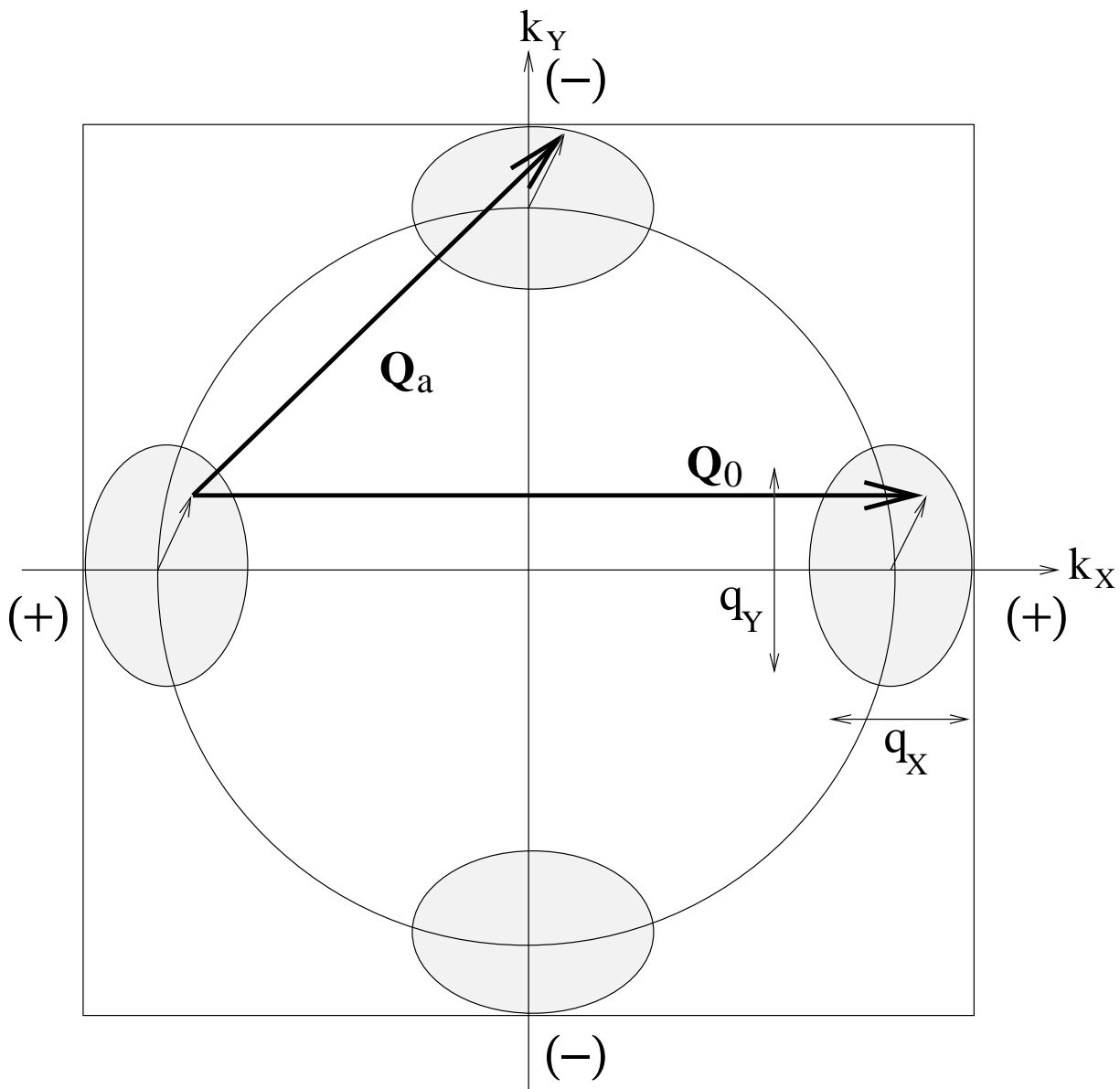


Fig. 2



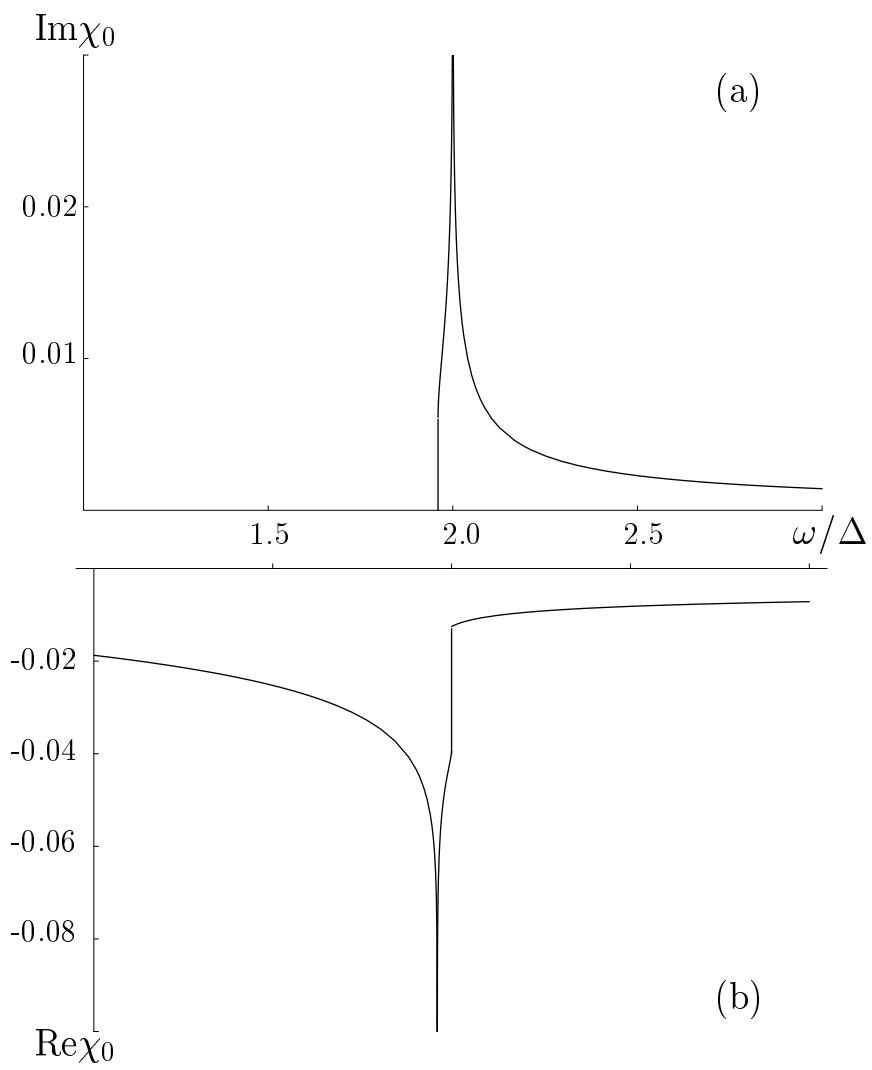


Fig. 3

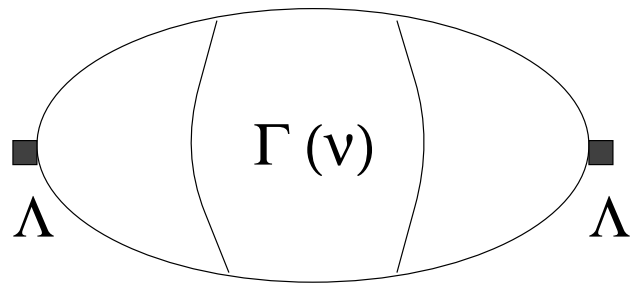
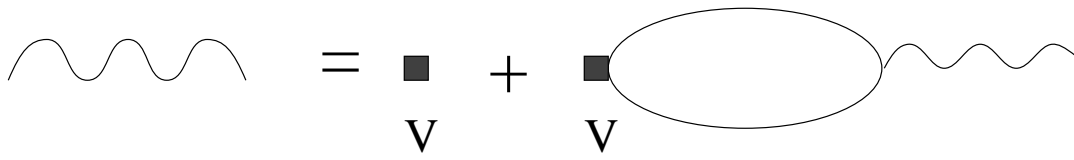
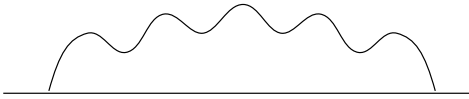


Fig. 4

(a)



(b)



(c)

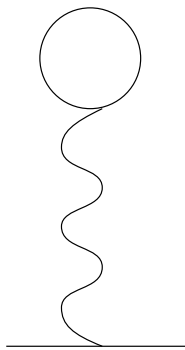


Fig. 5

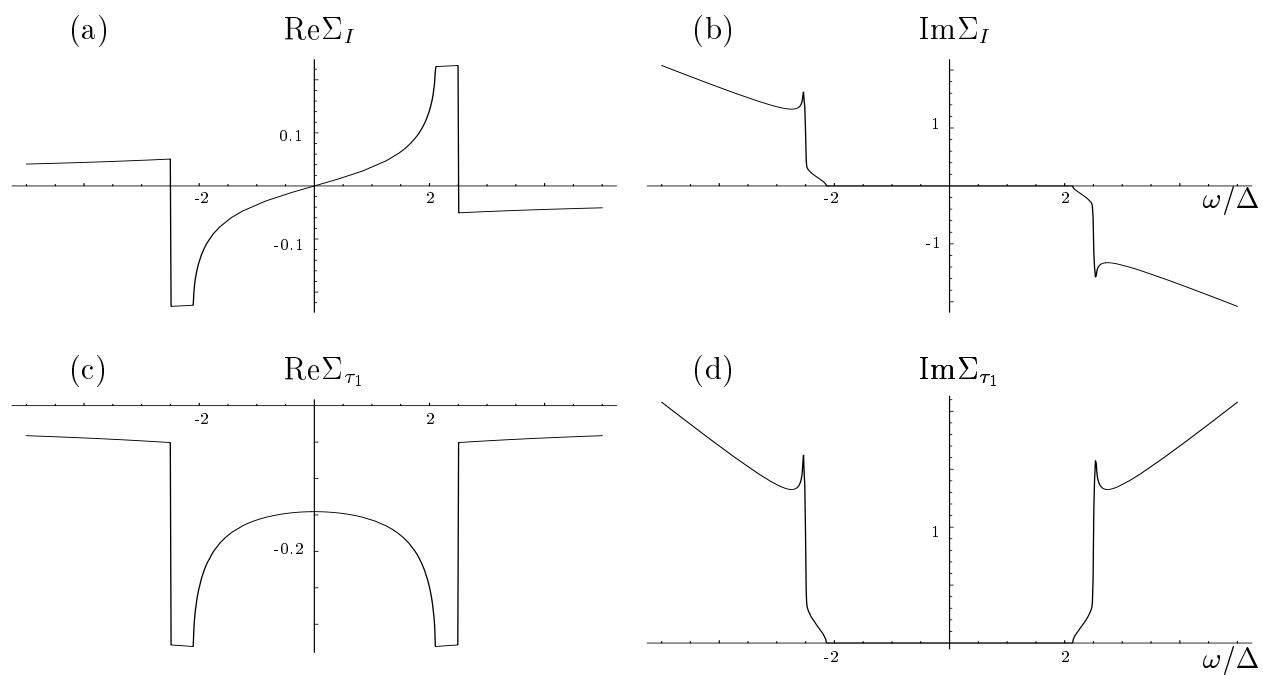


Fig. 6

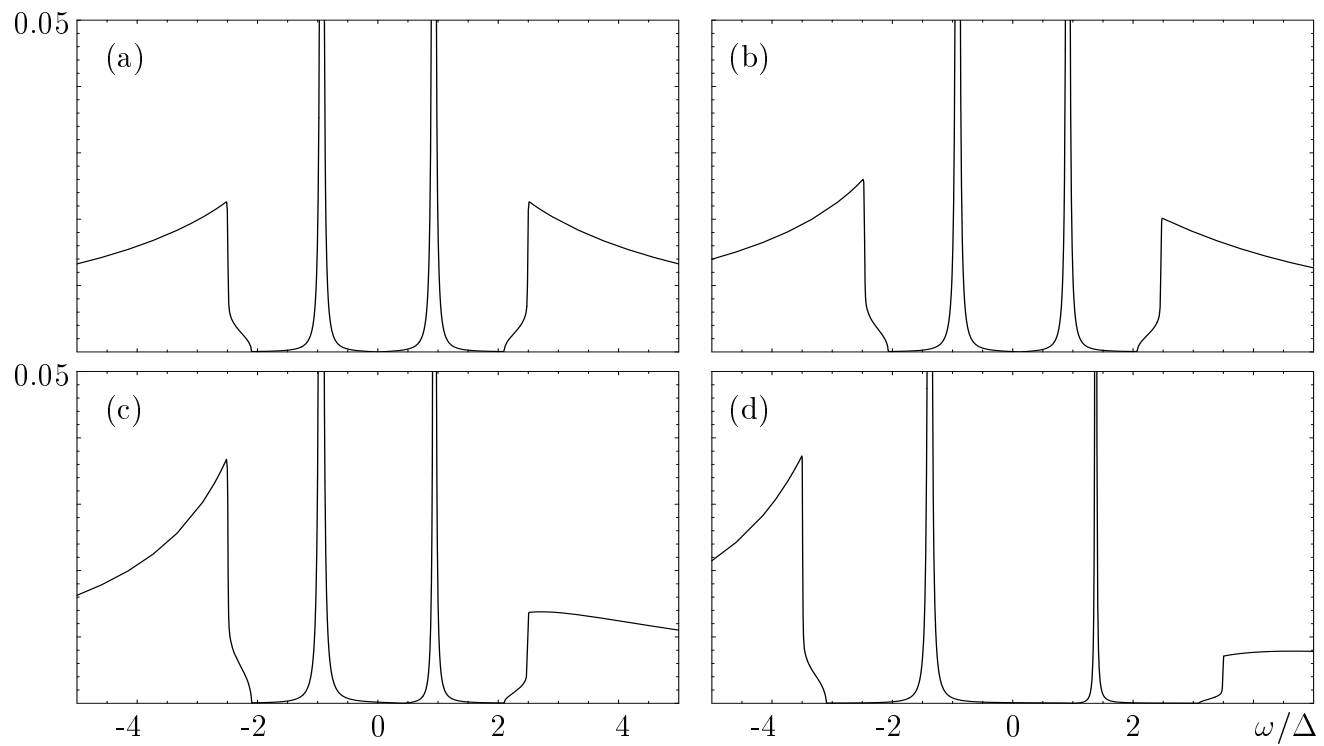


Fig. 7